ASME Journal of Applied Mechanics
Online journal at:
https://asmedigitalcollection.asme.org/appliedmechanics

A Cavity-Based Micromechanical Model for the Shear-Band Failure in Metallic Glasses Under Arbitrary Stress States

Yanfei Gao
Department of Materials Science and Engineering,
The University of Tennessee,
Knoxville, TN 37996
e-mail: ygao7@utk.edu

Deformation and fracture of metallic glasses are often modeled by stress-based criteria which often incorporate some sorts of pressure dependence. However, detailed mechanisms that are responsible for the shear-band formation and the entire damage initiation and evolution process are complex and the origin of such a pressure dependence is obscure. Here, we argue that the shear-band formation results from the constitutive instability, so that the shear-band angle and arrangements can be easily related to the macroscopic constitutive parameters such as internal friction and dilatancy factor. This is one reason for the observed tension-compression asymmetry in metallic glasses. The free volume coalescence leads to precipitous formation of voids or cavities inside the shear bands, and the intrinsic "ductility" is therefore governed by the growth of these cavities. Based on a generalized Stokes–Hookean analogy, we can derive the critical shear-band failure strain with respect to the applied stress triaxiality, in which the cavity evolution scenarios are sharply different between tension-controlled and shear/compression-dominated conditions. This is another possible reason for the tension-compression asymmetry. It is noted that diffusive-controlled cavity growth could also be the rate-determining process, as suggested by the recent measurements of shear-band diffusivity and viscosity that turn out to satisfy the Stokes–Einstein relationship. This constitutes the third possible reason for the tension-compression asymmetry. [DOI: 10.1115/1.4062724]

Keywords: shear-band failure strain, tension-compression asymmetry, cavity growth, failure criteria

1 Introduction

Owing to the amorphous nature of atomic packing, metallic glasses do not possess crystalline defects such as dislocations, so that they have some beneficial mechanical properties such as high strength and wear resistance. However, their inelastic response resembles brittle geomaterials; not only there is usually little or zero intrinsic ductility, but also the failure is preceded by strain localization into narrow bands that align closely with the principal shear directions [1,2]. Referring to the uniaxial test in Fig. 1(*a*), the shear band makes an angle of ~54 deg with respect to the loading axis in tension, or ~43 deg in compression. Numerous works have tried to rationalize this tension-compression asymmetry, with the most popular one being the Mohr–Coulomb analysis. Directly borrowing the form from that in geomechanics, we write

$$|\tau_s| + \mu\sigma_n = \tau_Y \tag{1}$$

where the shear stress on the shear-band plane is $\tau_s = \sigma \sin\theta \cos\theta$, the normal stress on the shear-band plane is $\sigma_n = \sigma \sin^2\theta$, τ_Y is the material yield strength, and μ is the coefficient of internal friction.

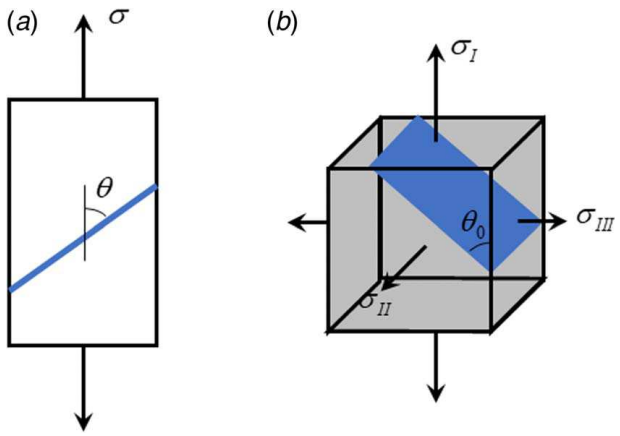

Fig. 1 The limited ductility in metallic glasses arises from the rapid initiation of strain localization into narrow bands (called shear bands as they align almost in the principal shear directions), and the subsequent transformation from shear bands to failure: (*a*) uniaxial loading condition and (*b*) shear band in the principal stress space with principal stresses sorted by $\sigma_I \geq \sigma_{II} \geq \sigma_{III}$

Manuscript received May 31, 2023; final manuscript received June 3, 2023; published online August 7, 2023. Assoc. Editor: Ruike Renee Zhao.

While the left-hand side reaches a maximum at an inclined angle that deviates from $\pi/4$ by $\pm\left[\frac{\pi}{2}-\frac{1}{2}\tan^{-1}(1/\mu)\right]$ for tension and compression, respectively, it only predicts the same deviation from $\pi/4$. Besides, Eq. (1) in geomechanics originates from the homogenization of collective behavior of many microcracks (or called shear faults) that are subjected to frictional sliding of the crack surfaces. There is no such counterpart mechanism in metallic glasses. What's more, the representation in Eq. (1) has been blindly adopted for the failure analysis of metallic glasses. The shear-band formation and the subsequent evolution into a shear failure indicate that a proper analysis should be based on the boundary value problem, rather than from a constitutive model like in Eq. (1). Consequently, in this work, we attempt to build up a mechanics model that capture the physical processes and provide the accurate analysis of the pressure dependence.

The shear-band formation is a constitutive instability, with the most common reasons including strain softening, non-associated flow, thermal softening, and others [3,4]. Because of the lack of one-to-one correspondence between stimuli and responses, there are multiple deformation paths, and the discontinuous bifurcation takes place from the homogeneous elastic-plastic deformation to the strain localization, inside which severe plastic deformation proceeds while outside which the material unloads elastically. For metallic glasses, one can adopt the Spaepen's free volume model where the free volume evolution provides a softening mechanism, or the modified version that includes thermal and/or free volume transport equations, or other structural state parameters than the free volume [5–7]. Regardless of the detailed model, the predicted shear band should not deviate much from the principal shear, as shown by the drawing in Fig. 1(*b*) with the highest shear achieved from $\frac{1}{2}(\sigma_{\rm I}-\sigma_{\rm III})$. While θ_0 is very close to 45 deg, Rudnicki and Rice [3] give its dependence on the macroscopic parameters, including internal friction μ and dilatancy factor β, by

$$\theta_0=\tan^{-1}\sqrt{\frac{\xi-N_{\min}}{N_{\max}-\xi}} \tag{2}$$

where $\xi=\frac{1}{3}(1+\nu)(\mu+\beta)-N(1-\nu)$, ν is Poisson's ratio, $N_{\min}=\sqrt{3}\sigma'_{\rm III}/\sigma_e$, $N=\sqrt{3}\sigma'_{\rm II}/\sigma_e$, $N_{\max}=\sqrt{3}\sigma'_{\rm I}/\sigma_e$, $\sigma'_{\rm I}$, $\sigma'_{\rm II}$, $\sigma'_{\rm III}$ are the principal deviatoric stresses, $\sigma_{\rm e}=\sqrt{\frac{3}{2}s_{ij}s_{ij}}$ is the Mises stress, and s_{ij} are the deviatoric stress tensor. Summation convention is implied for repeated Latin subscripts. The theoretical prediction in Eq. (2) can successfully reproduce the tension-compression asymmetry in the shear-band angle under uniaxial loading, if $\nu=0.3\sim0.4$ and $\mu+\beta=0.1\sim0.5$ [4].

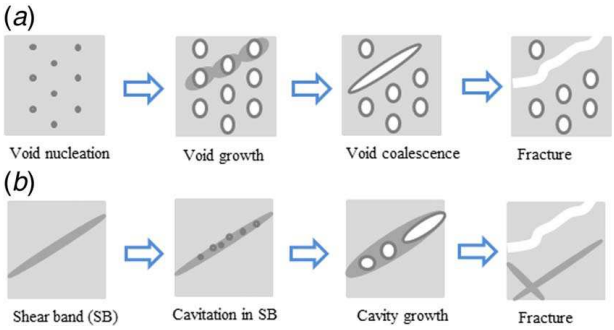

Fig. 2 Contrasting failure processes: (*a*) traditional metallic materials fail by the void nucleation, growth, and coalescence; and (*b*) metallic glasses first exhibit strain localizations, followed by cavitation processes inside the shear bands which eventually lead to fracture failure

Ductile fracture of crystalline metals involves the void nucleation, growth, coalescence into microcracks, and the eventual failure, as shown in Fig. 2(*a*). Several methodologies are generally employed, one being the damage mechanics approach such as the Gurson–Tvergaard–Needleman model [8], the other being the micromechanical cell model that explicitly embeds individual voids into the numerical simulations [9,10], and another class being the use of strain-based criteria [11], such as the Rice–Tracey criterion

$$\int_0^{\varepsilon_{\rm f}}\exp\left(c\frac{\sigma_{\rm m}}{\sigma_{\rm e}}\right)d\varepsilon=\text{const} \tag{3}$$

where $\varepsilon_{\rm f}$ is the critical failure strain, c is an unknown dimensionless parameter to be calibrated experimentally, and $\sigma_{\rm m}=\sigma_{\rm kk}/3$ is the mean stress. While these approaches have achieved great successes in material failure analysis, they cannot be directly adopted for metallic glasses, because the failure process should be described in Fig. 2(*b*). With a pre-existing crack, the failure of metallic glasses is governed by the competition between crack-tip shear-band formation and cleavage crack [2,12]. Without any pre-existing cracks, failures always start from shear bands by cavity nucleation and growth [13,14]. As shown by experimental observation in Li et al. [5] and theoretically analyzed in Wright et al. [6], shear-band formation in metallic glasses results into the free-volume oversaturation, which quickly leads to the nucleation of numerous nanometer-sized cavities. Consequently, it is the cavity growth and the subsequent microcrack formation that dictate the intrinsic "ductility," i.e., the maximum shear strain when an individual shear band can sustain prior to fracture failure. Qu et al. [14] employed 3D X-ray tomography to examine the evolution of shear-band cracking during compression test of $Zr_{65}Fe_5Al_{10}Cu_{20}$ metallic glass. Due to resolution limit, they only observed the evolution of microcracks on the shear-band plane before it fractures. These microcracks are elongated and then slightly kinked out of the normally flat shear-band plane, until they coalescence into larger microcracks. These observations provide the salient features on what could be the possible governing mechanisms for shear-band failure.

Based on the above discussions, this work aims to determine the critical condition for the catastrophic failure of an array of cavities (circular or lenticular or other shaped) lying on a narrow planar band. This problem resembles the intergranular creep fracture in polycrystalline materials at elevated temperatures [15–19]. As shown in Fig. 3(*a*), these cavities can grow due to the creep flow of the surrounding material or because of the diffusive process along the grain boundaries. In our problem, we have a shear band that has much higher shear strain rate than outside the shear band, and oftentimes the temperature inside is high so that the shear band behaves liquid like. How and what knowledge from intergranular creep fracture analysis can be transferred here will be thoroughly discussed in this paper.

2 Prediction Based on Creep-Constrained Cavity Growth

As explained in Introduction, the problem that dictates the failure process will be the growth of a planar array of cavities on the shear band, subjected to faraway applied stress fields. These cavities are nucleated from the unstable free volume field and quickly coalesce into feature sizes that are comparable to the shear-band thickness. Therefore, their growth should be controlled by the creeping response of the nearby material.

When the applied stress is shear or tension dominated, the anticipated cavity evolution will be schematically illustrated in Figs. 3(*b*) and 3(*c*), respectively. The boundary value problem in Fig. 3(*c*) has been simulated by Sham and Needleman [16] for grain boundary cavities in a power-law creeping solid. The growth of the cavity

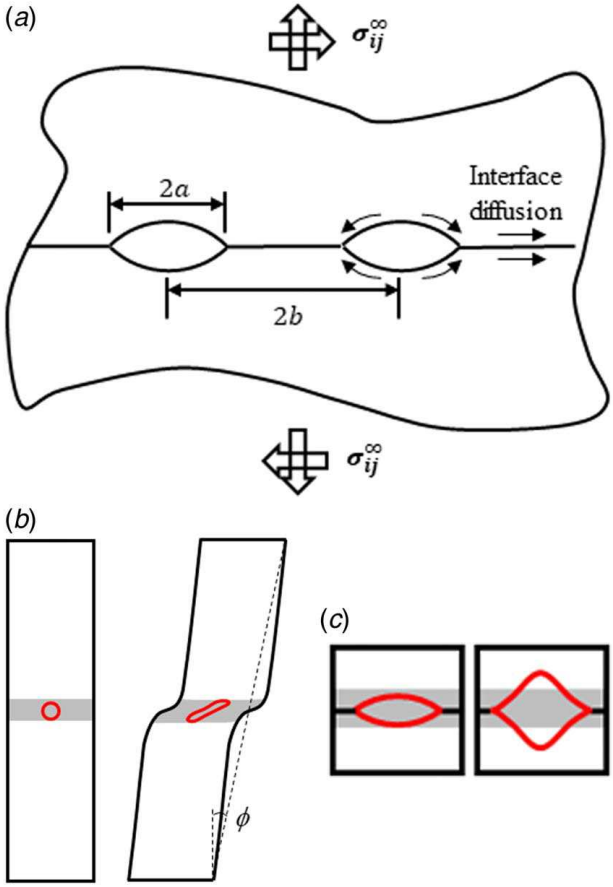

Fig. 3 (*a*) A distribution of cavities on a shear band plane can grow by creep deformation of the surrounding material, or by diffusive processes along the plane, (*b*) in pure shear, any shaped cavity inside the shear band will evolve sequentially as the following: flattened to a micro-crack, rotating and elongating into kinks, and then interacting with neighboring micro-cracks and eventually leading to coalescence, and (*c*) in tension, these cavities will grow and increase their volumes

density, as defined by $f_{\text{cavity}} = a^2/b^2$, is found to be

$$\frac{1}{f_{\text{cavity}}(1-f_{\text{cavity}})}\frac{df_{\text{cavity}}}{dt} = \dot{\varepsilon}^{\text{eff}}_{\text{creep}} \times F_{\text{Sham-Needleman}}(T, n) \tag{4}$$

$$F_{\text{Sham-Needleman}}(T, n) = \begin{cases} [\alpha_n |T| + \beta_n]^n \text{sgn}(T), & |T| > 1 \\ [\alpha_n + \beta_n]^n T, & |T| \le 1 \end{cases} \tag{5}$$

where $\dot{\varepsilon}^{\text{eff}}_{\text{creep}}$ is the effective creep strain rate (i.e., Mises form), sgn() is the sign function, and dimensionless parameters α_n and β_n are obtained from fitting to finite element simulations, given by

$$\alpha_n = \frac{3}{2n}, \quad \beta_n = \frac{(n-1)(n+0.4319)}{n^2} \tag{6}$$

The modified Sham–Needleman equation in Eq. (5) clearly shows the dependence on the stress triaxiality, $T = \sigma_{\text{m}}/\sigma_{\text{e}}$. We have added the term $1 - f_{\text{cavity}}$ to the left-hand side of Eq. (5), without which the original version in Ref. [16] only works when f_{cavity} is less than about 0.6.

If the applied T remains unchanged, the failure condition can be obtained by integrating Eq. (5),

$$\left[\ln\left(\frac{f_{\text{cavity}}}{1-f_{\text{cavity}}}\right)\right]_{f_0}^{f_{\text{final}}} = F_{\text{Sham-Needleman}} \int \dot{\varepsilon}^{\text{eff}}_{\text{creep}} dt \tag{7}$$

where the initial and final critical values of cavity are f_0 and f_{final}, respectively. If the mean stress is negative, i.e., $T < 0$, these cavities on the shear-band plane never grow so that the material becomes immortal, which is clearly not the reality. Nevertheless, we have a prediction of the shear-band failure strain, as given by

$$\varepsilon^{\text{sb}}_{\text{creep}}|_{\text{crt}} = \frac{c_1}{F_{\text{Sham-Needleman}}(T > 0, n)} = c_1 \times G_{\text{tension}}(T, n) \tag{8}$$

$$G_{\text{tension}}(T, n) = \begin{cases} \infty, & T \le 0 \\ \dfrac{1}{[\alpha_n + \beta_n]^n T}, & 0 < T \le 1 \\ \dfrac{1}{[\alpha_n T + \beta_n]^n}, & T > 1 \end{cases} \tag{9}$$

with a dimensionless parameter c_1 that needs to be calibrated with experiments. Here we write down the function G_{tension}, which is reciprocal to $F_{\text{Sham-Needleman}}$, for the sake of easy comparison to Eq. (12) as will be explained shortly.

If the applied loading condition is pure shear ($T = 0$) or shear/compression-dominated ($T < 0$), the modified Sham–Needleman model fails. Their simulations were performed mostly for $T > 1/3$, noting that the uniaxial tension corresponds to $T = 1/3$. Analytical solutions for two-dimensional circular or elliptical holes exist for linear elastic Hookean solid or Newtonian viscous material [20–23] and for perfectly plastic solids [24]. Even if we can follow the same solution approaches, these solutions are for small deformation and will not change the cavity closure result if $T < 0$. In shear/compression-dominated situations, as explained in Fig. 3(*b*), the cavities will be flattened out to micro-cracks, and then rotate and elongate until they interact with the neighboring micro-cracks. This is a large-deformation result that shows the long-term evolution of these cavities, which are only amenable to detailed finite element simulations.

It is certainly very tedious to conduct a full-field finite element simulation of cavity evolution under arbitrary T, especially when the loading condition is shear or compression dominated. This difficulty, however, can be bypassed by noting (i) the analogy between the initial value problem of a pure creeping solid under loads and the boundary value problem of a nonlinear elastic solid under the same loading conditions [25], and (ii) the extensive earlier works on computational cell model by Tvergaard and Nielsen [9]. If we replace all the rate measures in the creeping constitutive law by the non-rate ones in nonlinear elasticity (e.g., $\dot{\varepsilon}_{ij}$ by ε_{ij}), the governing equations for these two sets of constitutive models are identical. When the stress exponent $n = 1$, we see the analogy between Newtonian viscous material and Hookean elastic solid, which is also called Stokes–Hookean analogy. Furthermore, a nonlinear elasticity is the same as the deformation plasticity (i.e., proportional loading and no unloading). Tvergaard and Nielsen [9] have performed extensive finite element simulations of the cell model in Fig. 3(*b*) with the power-law plasticity, given in one-dimensional form by

$$\varepsilon_p = \frac{\sigma_{\text{Y}}}{E}\left(\frac{\sigma}{\sigma_{\text{Y}}}\right)^{1/N} \tag{10}$$

with the yield strength σ_{Y}, the Young's modulus E, and the working hardening exponent N. The above analogy leads to the same response of the cell model for a creeping solid with

$$\frac{\dot{\varepsilon}}{\dot{\varepsilon}_0} = \left(\frac{\sigma}{\sigma_0}\right)^n \tag{11}$$

with the stress exponent n and reference stress and strain rate, σ_0 and $\dot{\varepsilon}_0$, respectively. The analogy dictates that $n = 1/N$. Based on the above discussion, we denote this method as the generalized Stokes–Hookean analogy.

Representative finite element simulations in Fig. 4 exhibit the dependence of failure conditions on the stress triaxiality. In all these simulations, T is fixed as a constant, and the peak load

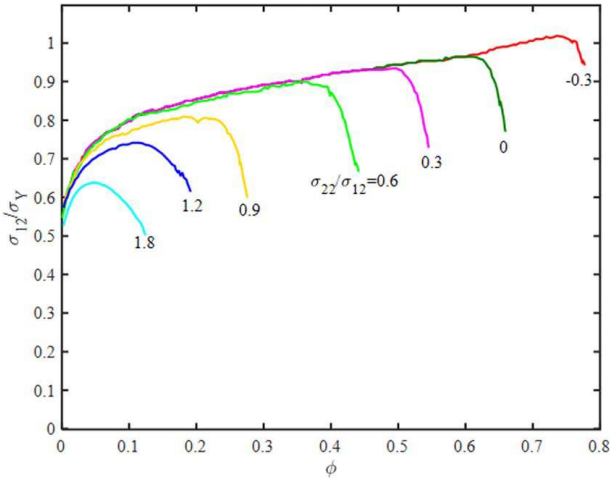

Fig. 4 For a power-law plastic solid, the response between the applied shear stress and the shear angle gives a clear failure that depends on the stress triaxiality. Finite element simulations of the boundary value problem in Fig. 3(*b*) are adapted from Fig. 2 in Tverggard and Nielsen [9] with $N = 0.1$.

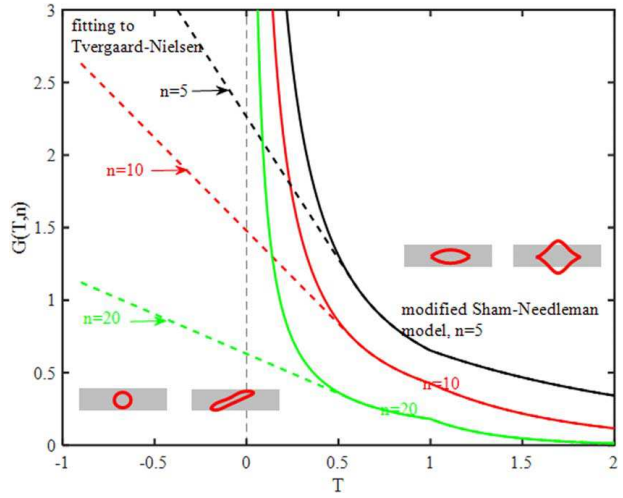

Fig. 5 Predicted critical shear strain for failure versus the stress triaxiality by the modified Sham–Needleman model in Eq. (9) and the modified Tvergaard–Nielsen model in Eq. (13). Schematic illustrations of the cavity evolution are shown in the insets. The diffusive model in Eq. (19) is not included.

corresponds to the flattening and rotation of the initial cavity, followed by the quick elongation into slit like cracks in the precipitous load drop stage. Although the generalized Stokes–Hookean analogy makes the correspondence between strain rates and strains, we note that the stress-triaxiality dependence of the failure process should be the same in both problems. In other words, there is no need for us to extend Sham–Needleman problems to the stress triaxiality range investigated by Ref. [9] A simple reading of the failure conditions with respect to the stress triaxiality will suffice. However, Tverggard and Nielsen [9] presented extensive results for $n = 10$, but only with a few data points for other n values. They also compared their computational cell model with respect to the modified Gurson model proposed by Nahshon and Hutchinson [8]. Although the agreement is only moderately satisfactory, this does provide additional results that complete a parametric study. These results should also agree with the Sham–Needleman results for $T > 1$. Our detailed fitting leads to the following results:

$$\varepsilon^{\text{sb}}_{\text{creep}}|_{\text{crt}} = c_2 \times G_{\text{shear}}(T, n) \tag{12}$$

$$G_{\text{shear}}(T, n) = \begin{cases} \dfrac{1}{(\alpha_n + \beta_n)^n}\left(2\sqrt{3} - 3T\right), & T < \dfrac{1}{\sqrt{3}} \\ \dfrac{1}{(\alpha_n + \beta_n)^n T}, & \dfrac{1}{\sqrt{3}} \le T < 1 \\ \dfrac{1}{(\alpha_n T + \beta_n)^n}, & T \ge 1 \end{cases} \tag{13}$$

with dimensionless parameters α_n and β_n given in Eq. (6). When using this criterion, it should be noted that the critical strain should be assessed for the shear band, and the unknown dimensionless parameter c_2 should be calibrated from experimental comparisons.

Predictions in Eqs. (9) and (13) are plotted in Fig. 5 for representative n values, which provides an explanation of the tension-compression asymmetry of "intrinsic ductility" in metallic glasses. It should be reminded that the shear band angle only shows a very weak dependence on the stress state, as explained in the Introduction. In contrast, metallic glasses show little ductility under tension, but moderate ductility under compression. According to Fig. 5, under tension-dominated loading conditions (i.e., $T > 1/3$), there is an inverse dependence of shear-band failure strain on T. When the applied stress is shear/compression dominated (e.g., $T < 0$), the complex evolution of cavities from flattening, rotating, elongating, and coalescing leads to considerable critical strain for failure. This can only be properly explained in Eq. (13), as opposed to the modified Sham–Needleman model in Eq. (9).

3 Prediction Based on Diffusion-Controlled Cavity Growth

In the high temperature failures of polycrystalline materials, it is well known that grain boundary diffusive processes can be responsible for the cavity growth. As shown in Fig. 3(*a*), the applied normal stress changes the chemical potential by $-\Omega\sigma_n$ with the atomic volume Ω. This causes a gradient in chemical potential and thus drives the surface and interface diffusion that enlarges the cavity volume. Following Hull and Rimmer [26] and Cocks and Ashby [27], we write down the evolution equation as

$$\frac{df_{\text{cavity}}}{dt} = \frac{2f_{\text{cavity}}}{a^3 \ln(1/f_{\text{cavity}})} \frac{D_{\text{sb}}\delta_{\text{sb}}\Omega}{k_{\text{B}}T_{\text{K}}}\sigma_n \tag{14}$$

where D_{sb} is the self-diffusivity along the shear band, δ_{sb} is the shear band thickness, k_{B} is the Boltzmann constant, and T_{K} is the absolute temperature in Kelvin. It is a daunting task to measure the shear-band diffusivity. One of such rare successes is presented by the work of Bokeloh et al. [28], which employs the tracer measurements by using a radioactive isotope. For $Pd_{40}Ni_{40}P_{20}$ metallic glass, they found out that the shear band diffusivity is $D_{\text{sb}} = (1.13 \sim 1.96) \times 10^{-17}\text{m}^2/\text{s}$ and the shear band viscosity is $\eta_{\text{sb}} = (0.11 \sim 5.3) \times 10^5\text{Pa} \cdot \text{s}$. Song and Nieh [29] and Wright et al. [30] used high-speed camera and captured the dynamic response of shear-band propagation, and found out that the shear-band viscosity is $\eta_{\text{sb}} = (2 \sim 7) \times 10^4\text{Pa} \cdot \text{s}$ for Vitreloy 1 and $\eta_{\text{sb}} = (0.11 \sim 5.3) \times 10^5\text{Pa} \cdot \text{s}$ for Zr-based metallic glasses. While shear band diffusivity is not known in these works, their viscosity measurements agree well with theoretical models by Ref. [7], which suggests the existence of high temperature and liquid-like behavior inside the shear bands. These measurements actually satisfy the classic Stokes–Einstein relationship

$$D_{\text{sb}} = \frac{k_{\text{B}}T_{\text{K}}}{6\pi\eta_{\text{sb}}R} \tag{15}$$

where R is atomic radius. Therefore, the doubts on the order of magnitude of their measured viscosity by Bokeloh et al. [28] are not warranted, because of this relationship.

A question that naturally arises is the effect of diffusive process on the cavity growth, in relative to the creep processes. Following Needleman and Rice [15], a comparison between Eqs. (4) and (14) defines a length scale

$$L_{\text{Needleman}-\text{Rice}} = \left[\frac{D_{\text{sb}}\delta_{\text{sb}}\Omega}{k_{\text{B}}T_{\text{K}}}\cdot\frac{\sigma_{\text{e}}}{\dot{\varepsilon}^{\text{ext}}_{\text{creep}}}\right]^{1/3} \tag{16}$$

where the superscript "ext" emphasizes the creep strain rate is that of the surrounding material. Note that the viscosity of the surrounding material is $\eta_{\text{ext}} = \sigma_e/3\dot{\varepsilon}^{\text{ext}}_{\text{creep}}$. Taking shear-band diffusivity of 10^{-17} m^2/s and external viscosity of 10^{11} Pa·s, this length scale will be about 20 nm. While diffusive process inside the shear band is of atomic scale as justified by the Stokes–Einstein relationship, the above Needleman–Rice length scale amplifies the diffusive contribution to cavity growth for cavities of tens of nanometers in size. Therefore, the early stage of cavity growth under tension-dominated stress state is governed by both creep and diffusive processes, while later stage is purely by creep-constrained cavity growth. Substituting Eq. (15) into Eq. (16) gives an alternative representation, $L_{\text{Needleman}-\text{Rice}} = \left[\frac{\delta_{\text{sb}}\Omega}{2\pi R}\cdot\frac{\eta_{\text{ext}}}{\eta_{\text{sb}}}\right]^{1/3}$, so that the cavity growth equation in Eq. (14) can be rewritten as

$$\begin{aligned}\frac{df_{\text{cavity}}}{dt} &= \frac{2f_{\text{cavity}}}{\ln(1/f_{\text{cavity}})}\dot{\varepsilon}^{\text{ext}}_{\text{creep}}\left(\frac{\sigma_{\text{n}}}{\sigma_{\text{e}}}\right)\left(\frac{L_{\text{Needleman}-\text{Rice}}}{a}\right)^3 \\ &= \frac{2f_{\text{cavity}}}{\ln(1/f_{\text{cavity}})}\frac{2\delta_{\text{sb}}R^2}{3a^3}\frac{\sigma_{\text{n}}}{\sigma_{\text{e}}}\dot{\varepsilon}^{\text{sb}}_{\text{creep}}\end{aligned} \tag{17}$$

Following the same operations that derive the failure criteria in Eqs. (8) and (12), we write down the critical strain for shear-band failure as

$$\varepsilon^{\text{sb}}_{\text{creep}}|_{\text{crt}} = c_3 \times G_{\text{diffusion}}(T) \tag{18}$$

$$G_{\text{diffusion}}(T) = \begin{cases}\infty, & T<0\\ \dfrac{1}{T}, & T\geq 0\end{cases} \tag{19}$$

where the dimensionless parameter c_3 needs to be calibrated from experiments.

The forms of $G_{\text{diffusion}}(T)$ and $G_{\text{tension}}(T, n)$ are similar, while c_1 mainly depends on initial value of f_{cavity} and c_3 additionally on the initial cavity size (i.e., the value of $a^3/(\delta_{\text{sb}}R^2)$). For this reason, $G_{\text{diffusion}}(T)$ is not plotted on Fig. 5. When the cavities are small, the concerted contributions from both diffusive processes and creep deformation could lead to a very fast growth rate, so that the resulting intrinsic ductility can be very small. For shear/compression-dominated loading conditions, $T<0$ and the applied normal stress is negative. The Hull–Rimmer process shall not contribute to the cavity growth; in fact, the compressive normal stress will lead to cavity closure—a process denoted as solid-state bonding [31]. Consequently, the diffusive-controlled cavity growth provides yet another reason for the tension-compression asymmetry of "intrinsic ductility" in metallic glasses.

4 Summary

Because the free volume field inside the shear band is highly unstable and quickly leads to the nucleation of nanometer-sized cavities, it is the cavity growth that dictates the intrinsic ductility, namely, the critical strain that the shear band can sustain prior to its transition into fracture failure. Prior studies on intergranular creep fracture are incomplete for small and negative T values. Noting the generalized Stokes–Hookean analogy, this work is able to present a comprehensive description of the dependence of the shear-band failure strain on T. The cavity evolution under shear/compression-dominated stress states provides a mechanistic explanation of the contrasting ductility under tension versus compression conditions. The contribution from diffusive processes offers another complementary scenario for cavity growth.

Acknowledgment

The author would like to dedicate this work to Professor Kyung-Suk Kim at Brown University for the occasion of his 70th birthday and in this special issue that honors his contributions in nano-, bio-, and fracture mechanics across a wide range of spatiotemporal scales. Financial support is provided by the National Science Foundation (IIP 2052729).

Conflict of Interest

The author declares that there are no known competing financial interests or personal relationships that could have appeared to influence the work reported in this paper.

Data Availability Statement

Data contained in this paper are available upon request to the corresponding author.

References

[1] Sun, B. A., and Wang, W. H., 2015, "The Fracture of Bulk Metallic Glasses," Prog. Mater. Sci., **74**, pp. 211–307.
[2] Jia, H. L., Wang, G. Y., Chen, S. Y., Gao, Y. F., Li, W. D., and Liaw, P. K., 2018, "Fatigue and Fracture Behavior of Bulk Metallic Glasses and Their Composites," Prog. Mater. Sci., **98**, pp. 168–248.
[3] Rudnicki, J. W., and Rice, J. R., 1975, "Conditions for the Localization of Deformation in Pressure-Sensitive Dilatant Materials," J. Mech. Phys. Solids, **23**(6), pp. 371–394.
[4] Gao, Y. F., Wang, L., Bei, H., and Nieh, T. G., 2011, "On the Shear-Band Direction in Metallic Glasses," Acta Mater., **59**(10), pp. 4159–4167.
[5] Li, J., Spaepen, F., and Hufnagel, T. C., 2002, "Nanometre-Scale Defects in Shear Bands in a Metallic Glass," Philos. Mag., **82**(13), pp. 2623–2630.
[6] Wright, W. J., Hufnagel, T. C., and Nix, W. D., 2003, "Free Volume Coalescence and Void Formation in Shear Bands in Metallic Glass," J. Appl. Phys., **93**(3), pp. 1432–1437.
[7] Lu, J., Ravichandran, G., and Johnson, W. L., 2003, "Deformation Behavior of the $Zr_{41.2}Ti_{13.8}Cu_{12.5}Ni_{10}Be_{22.5}$ Bulk Metallic Glass Over a Wide Range of Strain-Rates and Temperatures," Acta Mater., **51**(12), pp. 3429–3443.
[8] Nahshon, K., and Hutchinson, J. W., 2008, "Modification of the Gurson Model for Shear Failure," Eur. J. Mech. A Solids, **27**(1), pp. 1–17.
[9] Tvergaard, V., and Nielsen, K. L., 2010, "Relations Between a Micro-Mechanical Model and a Damage Model for Ductile Failure in Shear," J. Mech. Phys. Solids, **58**(9), pp. 1243–1252.
[10] Cui, Y., Gao, Y. F., and Chew, H. B., 2020, "Two-Scale Porosity Effects on Cohesive Crack Growth in a Ductile Media," Int. J. Solids Struct., **200–201**, pp. 188–197.
[11] Barnwal, V. K., Lee, S.-Y., Choi, J., Kim, J.-H., and Barlat, F., 2021, "Performance Review of Various Uncoupled Fracture Criteria for TRIP Steel Sheet," Int. J. Mech. Sci., **195**, p. 106269.
[12] Jiang, M. Q., Ling, Z., Meng, J. X., and Dai, L. H., 2008, "Energy Dissipation in Fracture of Bulk Metallic Glasses Via Inherent Competition Between Local Softening and Quasi-Cleavage," Philos. Mag., **88**(3), pp. 407–426.
[13] Huang, X., Ling, Z., and Dai, L. H., 2013, "Cavitation Instabilities in Bulk Metallic Glasses," Int. J. Solids Struct., **50**(9), pp. 1364–1372.
[14] Qu, R. T., Wang, S. G., Wang, X. D., Liu, Z. Q., and Zhang, Z. F., 2017, "Revealing the Shear Band Cracking Mechanism in Metallic Glass by X-ray Tomography," Scr. Mater., **133**, pp. 24–28.
[15] Needleman, A., and Rice, J. R., 1980, "Plastic Creep Flow Effects in the Diffusive Cavitation of Grain Boundaries," Acta Metall., **28**(10), pp. 1315–1332.
[16] Sham, T.-L., and Needleman, A., 1983, "Effects of Triaxial Stressing on Creep Cavitation of Grain Boundaries," Acta Metall., **31**(6), pp. 919–926.
[17] Zhang, W., Wang, X., Wang, Y., Yu, X., Gao, Y., and Feng, Z., 2020, "Type IV Failure in Weldment of Creep Resistant Ferritic Alloys: I. Micromechanical Origin of Creep Strain Localization in the Heat Affected Zone," J. Mech. Phys. Solids, **134**, p. 103774.
[18] Zhang, W., Wang, X., Wang, Y., Yu, X., Gao, Y., and Feng, Z., 2020, "Type IV Failure in Weldment of Creep Resistant Ferritic Alloys: II. Creep Fracture and Lifetime Prediction," J. Mech. Phys. Solids, **134**, p. 103775.
[19] Zhang, W., Gao, Y. F., Feng, Z. L., Wang, X., Zhang, S., Huang, L., Huang, Z. W., and Jiang, L., 2020, "Ductility Limit Diagrams for Superplasticity and Forging of High Temperature Polycrystalline Materials," Acta Mater., **194**, pp. 378–386.

[20] McClintock, F. A., Kaplan, S. M., and Berg, C. A., 1966, "Ductile Fracture by Hole Growth in Shear Band," Int. J. Fracture Mech., **2**(4), pp. 614–627.
[21] McClintock, F. A., 1968, "A Criterion for Ductile Fracture by the Growth of Holes," ASME J. Appl. Mech., **35**(2), pp. 363–371.
[22] Fleck, N. A., and Hutchinson, J. W., 1986, "Void Growth in Shear," Proc. R. Soc. Lond. A, **407**(1833), pp. 435–458.
[23] Fleck, N. A., Hutchinson, J. W., and Tvergaard, V., 1989, "Softening by Void Nucleation and Growth in Tension and Shear," J. Mech. Phys. Solids, **37**(4), pp. 515–540.
[24] Anderson, P. M., Fleck, N. A., and Johnson, K. L., 1990, "Localization of Plastic Deformation in Shear Due to Microcracks," J. Mech. Phys. Solids, **38**(5), pp. 681–699.
[25] Bower, A. F., Fleck, N. A., Needleman, A., and Ogbonna, N., 1993, "Indentation of a Power Law Creeping Solid," Proc. R. Soc. Lond. Ser., A: Math. Phys. Sci., **441**(1911), pp. 97–124.
[26] Hull, D., and Rimmer, D. E., 1959, "The Growth of Grain-Boundary Voids Under Stress," Philos. Mag., **4**(42), pp. 673–687.
[27] Cocks, A. C. F., and Ashby, M. F., 1982, "On Creep Fracture by Void Growth," Prog. Mater. Sci., **27**(3–4), pp. 189–244.
[28] Bokeloh, J., Divinski, S. V., Reglitz, G., and Wilde, G., 2011, "Tracer Measurements of Atomic Diffusion Inside Shear Bands of a Bulk Metallic Glass," Phys. Rev. Lett., **107**(23), p. 235503.
[29] Song, S. X., and Nieh, T. G., 2009, "Flow Serration and Shear-Band Viscosity During Inhomogeneous Deformation of a Zr-Based Bulk Metallic Glass," Intermetallics, **17**(9), pp. 762–767.
[30] Wright, W. J., Samale, M. W., Hufnagel, T. C., LeBlanc, M. M., and Florando, J. N., 2009, "Studies of Shear Band Velocity Using Spatially and Temporally Resolved Measurements of Strain During Quasistatic Compression of a Bulk Metallic Glass," Acta Mater., **57**(16), pp. 4639–4648.
[31] Wang, X., Gao, Y., McDonnell, M., and Feng, Z., 2022, "Determination of the Friction Stir Welding Window From the Solid-State-Bonding Mechanics Under Severe Thermomechanical Conditions," Materialia, **21**, p. 101350.